

01 May 2018

Elucidating the Effect of Water-To-Cement Ratio on the Hydration Mechanisms of Cement

Aida Margarita Ley-Hernandez

Jonathan Lapeyre


Rachel Cook

Aditya Kumar

Missouri University of Science and Technology, kumarad@mst.edu

et. al. For a complete list of authors, see https://scholarsmine.mst.edu/matsci_eng_facwork/2374

Follow this and additional works at: https://scholarsmine.mst.edu/matsci_eng_facwork

 Part of the [Civil and Environmental Engineering Commons](#), and the [Materials Science and Engineering Commons](#)

Recommended Citation

A. M. Ley-Hernandez et al., "Elucidating the Effect of Water-To-Cement Ratio on the Hydration Mechanisms of Cement," *ACS Omega*, vol. 3, no. 5, pp. 5092-5105, American Chemical Society (ACS), May 2018.

The definitive version is available at <https://doi.org/10.1021/acsomega.8b00097>

This Article - Journal is brought to you for free and open access by Scholars' Mine. It has been accepted for inclusion in Materials Science and Engineering Faculty Research & Creative Works by an authorized administrator of Scholars' Mine. This work is protected by U. S. Copyright Law. Unauthorized use including reproduction for redistribution requires the permission of the copyright holder. For more information, please contact scholarsmine@mst.edu.



Elucidating the Effect of Water-To-Cement Ratio on the Hydration Mechanisms of Cement

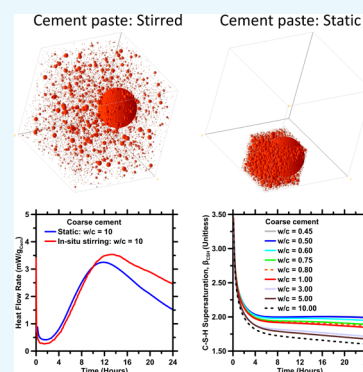
Aida Margarita Ley-Hernandez,[†] Jonathan Lapeyre,[‡] Rachel Cook,[§] Aditya Kumar,^{*,||} and Dimitri Feys[⊥]

[†]Department of Civil, Architectural, and Environmental Engineering, [‡]Department of Materials Science and Engineering,

[§]Department of Materials Science and Engineering, ^{||}Department of Materials Science and Engineering, and [⊥]Department of Civil, Architectural, and Environmental Engineering, Missouri University of Science and Technology (S&T), Rolla, Missouri 65409-0340, United States

Supporting Information

ABSTRACT: The hydration of cement is often modeled as a phase boundary nucleation and growth (pBNG) process. Classical pBNG models, based on the use of isotropic and constant growth rate of the main hydrate, that is, calcium–silicate–hydrate (C–S–H), are unable to explain the lack of any significant effect of the water-to-cement (w/c) ratio on the hydration kinetics of cement. This paper presents a modified form of the pBNG model, in which the anisotropic growth of C–S–H is allowed to vary in relation to the nonlinear evolution of its supersaturation in solution. Results show that once the supercritical C–S–H nuclei form, their growth remains confined within a region in proximity to the cement particles. This is hypothesized to be a manifestation of the sedimentation of cement particles, which imposes a space constraint for C–S–H growth. In pastes wherein the sedimentation of cement particles is disrupted, the hydration kinetics are no longer unresponsive to changes in w/c . Unlike C–S–H, the ions in solution are not confined, and hence, the supersaturation-dependent growth rate of C–S–H diminishes monotonically with increasing w/c . Overall, the outcomes of this work highlight important aspects that need to be considered in employing pBNG models for simulating hydration of cement-based systems.



INTRODUCTION

The reaction between cement and water, that is, hydration, involves dissolution of the anhydrous phases concomitant with precipitation of the hydration products (subsequently referred to as hydrates). Extensive research has been devoted to study the kinetics of cement hydration, as it principally dictates the development of the microstructure and the consequent evolution of both fresh (e.g., workability and time of set) and hardened properties (e.g., the rate/extent of strength development) of concrete.^{1–3} It is widely accepted^{1,2,4–6} that the early stage of cement hydration is driven by the nucleation and growth^{7–10} of the main hydration product, that is, calcium–silicate–hydrate^{1,5,11–13} (C–S–H, as per cement chemistry notation: C = CaO, S = SiO₂, H = H₂O, A = Al₂O₃, and F = Fe₂O₃); although, it is worth mentioning that in some studies,^{14,15} it has been argued that kinetics of cement hydration is controlled by dissolution of the phases present in cement. In a typical plain cement paste (i.e., cement + water), C–S–H nucleates heterogeneously on the solid-phase boundaries, that is, surfaces of cement particles, and therefore, the mechanism of its formation is usually termed as phase boundary nucleation and growth (pBNG). As hydration progresses, the percolation of the overlapping layers of C–S–H binds the paste cohesively and leads to setting and subsequent development of mechanical properties.^{5,11,16,17} Akin to pBNG processes occurring in metallic systems (e.g., solidification of metal),^{18,19} the temporal evolution of cement

hydration rate, as monitored using isothermal calorimetry techniques, comprises a characteristic reaction rate peak (i.e., the main hydration peak) up to which the rate of reaction accelerates and beyond which it declines.^{1,13}

Several numerical models based on the pBNG mechanism have been developed to reproduce the experimental measurements of cement hydration rates.^{5,6,11,12,16,20,21} In these models, a single product of constant density is assumed to form heterogeneously on solid phase boundaries at a given nucleation event, and its subsequent growth into the contiguous capillary pore space is treated as the rate-controlling mechanism. As the product fills up the capillary pore space, impingements between product nuclei, growing on the same or adjacent anhydrous particles, become increasingly dominant and ultimately cause a deceleration in the overall hydration rate. Numerical models, based on this premise and some additional assumptions (e.g., spherical or needlelike geometry of the product, diffusion-limited kinetics at later ages, and time-dependent growth of C–S–H) have successfully been used to fit the hydration rates of cementitious systems.^{5,6,12,16,20–24} These fits are typically obtained by iteratively varying relevant pBNG parameters (e.g., nucleation site frequency and product growth rate) to minimize the deviation between numerical and

Received: January 16, 2018

Accepted: April 27, 2018

Published: May 9, 2018

experimental hydration rates. However, as pointed out,^{6,22,25} the parameters derived from such a fitting can be misleading as some underlying assumptions of the classical pBNG mechanism do not necessarily represent the physics of C–S–H nucleation and growth accurately. More specifically, the assumptions of (a) isotropic (i.e., spherical) growth of the product does not represent the experimentally observed needlelike geometry of C–S–H growth at early ages,^{26–28} (b) the constant rate of product growth does not comply with the time-dependent variation of its supersaturation in the solution,^{13,22,27,29,30} and (c) unconstrained formation of the product throughout the capillary pore space fails to explain the lack of any significant effect of the water-to-cement ratio (w/c mass basis) on the hydration kinetics of cement.^{16,31,32} The last point is the main focus of this study and is described in further detail below.

Past studies^{12,16,31} have shown that the early age (i.e., up to 24 h) hydration kinetics of cement are broadly unaffected by the w/c of the system. However, in pBNG models,^{6,16,25,32} an increase in w/c implies a decrease in the area of the substrate per unit volume of the paste, which in turn affects the rate of formation of C–S–H and thus the overall hydration kinetics. Specifically, with increasing w/c , whereas impingements between C–S–H nuclei growing on the same particle remain broadly unaffected (i.e., assuming the same nucleation density of C–S–H), impingements between C–S–H layers growing on adjacent cement particles are fewer because of larger spacing between them. As a result, pBNG models predict a dependency of the hydration rate on w/c , unlike what is observed in experiments.^{12,16,31} These contradictions between experimentally observed hydration rates and predictions of the pBNG model, including ones that involve the implementation of the nucleation and densifying growth theory (i.e., time-dependent densification of C–S–H),^{5,16,33} are highlighted in the work of Kirby and Biernacki.³¹ In a recent study, Masoero et al.³⁴ proposed a *reaction zone* hypothesis to reconcile the aforementioned contradictions. The authors proposed that during the early hydration period, C–S–H grows exclusively within regions close to surfaces of the reactant particles; these regions collectively were designated as the reaction zone. Within the reaction zone, as the amount of C–S–H increases with hydration, growing impingements between C–S–H nuclei causes deceleration of the hydration rate, all while abundant capillary pore space remains unoccupied outside of the reaction zone. The hypothesis provides novel and significant insights and, more importantly, explains the mechanisms driving the deceleration of the hydration rate beyond the main hydration peak in high w/c systems. However, the assumption of the growth rate of C–S–H being constant throughout the process of hydration, as used in the study,³⁴ is inconsistent with recent studies that clearly show a temporal decline of C–S–H supersaturation (i.e., driving force for the growth of C–S–H) in solution.^{22,27,29,30} In addition, Masoero et al.³⁴ assumed the growth of C–S–H to occur at equivalent rates in all directions. This assumption has implications not just on the geometry of C–S–H nuclei but also on the overall rate of hydration. Scherer et al.^{6,28} noted that at early stages of cement hydration, the growth of C–S–H occurs in a highly anisotropic manner. Specifically, the growth rate of C–S–H in the direction normal to and away from the substrate is higher than its growth rate in the direction parallel to the substrate. This theory of anisotropic growth of C–S–H gains support from recent microscopic observations of the geometry of C–S–H growth.^{26–28} Assuming isotropic growth of C–S–H also results in greater

impingements of its nuclei and, thus, a faster approach to the main hydration peak.^{6,25} As a result of these discrepancies between experiments and assumptions made within the model presented in ref 34, the pBNG parameters derived from the simulations are difficult to interpret. As examples, the predictions of (i) significantly higher nucleation density of C–S–H in C_3S (i.e., tricalcium silicate, the major phase in cement constituting 50–70% of its mass³) suspensions (i.e., $w/c = 50$) as compared to that in pastes (i.e., $w/c = 0.40$)³⁴ are difficult to reconcile considering that the critical supersaturation at which nucleation of C–S–H occurs should be independent of the w/c ,^{5,22,35} and (ii) the smaller size of the reaction zone in suspensions as compared to that in pastes³⁴ is counterintuitive, considering that the capillary pore space increases with increasing w/c , thus allowing C–S–H to grow more freely. To resolve these inconsistencies and to better explain the role of w/c on the mechanisms of cement hydration, further refinement of the pBNG model is needed. Such refinements need to be based on observations from experiments reported in various recent studies.^{26,27}

This study employs a combination of experiments and computer simulations to elucidate the effect of w/c on the early age hydration kinetics of cement. Isothermal microcalorimetry is used to measure the hydration rates of cementitious systems across a wide range of w/c , including both pastes and suspensions. A pBNG model, incorporating a modification of the reaction zone hypothesis and allowing anisotropic and time-dependent growth rate of the hydrate, is developed and tested against experiments. Results obtained are used to describe the mechanisms that drive the progress of nucleation and growth of the C–S–H in such systems. The outcomes provide new understanding and quantification of rate controls of cement hydration and highlight important aspects pertaining to pBNG processes that need to be considered in the development of numerical pBNG models.

■ PBNG MODEL

A modified pBNG formulation is applied to describe the effects of w/c on the hydration kinetics of cement. The cement used in our study is composed of four phases (C_3S , C_2S , C_3A , and C_4AF), all of which react with water simultaneously, though at different rates.¹ C_2S and C_4AF have low intrinsic dissolution rates and, hence, do not release substantial amounts of heat at early ages.^{1,6,14} In contrast to these phases, the reaction of C_3A with water and aqueous SO_4^{2-} ions (i.e., resulting from the dissolution of gypsum) is rapid; this causes nucleation of ettringite crystals within the first few minutes of mixing.^{36,37} Nonetheless, after the initial nucleation burst, ettringite subsequently grows at a very slow (and near constant) rate for the next few hours, thus releasing little heat.^{36,38} As such, in pBNG models applied to cement pastes,^{6,11,12,16,25,39} including the model used herein, early age kinetics of cement hydration is assumed to be dominated by hydration of the C_3S phase. The same assumption implies that during the early stages of cement hydration, the major products in the cement paste are C–S–H and CH, both of which form in stoichiometric amounts in relation to the amount of hydrated C_3S . On the basis of these assumptions, in pBNG models, a single product of constant density (i.e., combining the bulk density of CH and C–S–H phases) is assumed to form at a given nucleation event, and its subsequent growth on solid-phase substrate boundaries (i.e., cement surfaces) is treated as the rate-controlling mechanism that drives the kinetics during the early ages of cement

hydration. This assumption is referred to as the *site saturation condition*, implying that the growth of the product phase begins from a fixed number of nuclei that form at very early ages (i.e., at time = τ h), and no further nuclei are permitted to form after this very initial nucleation burst^{40,41} (i.e., nucleation rate = $0 \mu\text{m}^{-2}\cdot\text{h}^{-1}$). On the basis of these criteria, at any given time t (h), the volume fraction of the reactants (i.e., C_3S and water) transformed to product [$X(t)$, unitless: volume of product divided by the total initial volume of the paste] is given by eq 1.^{13,22,25,35,42}

$$X(t) = 1 - \exp\left[-2k_G \cdot (t - \tau) \cdot \left(1 - \frac{F_D[k_s \cdot (t - \tau)]}{k_s \cdot (t - \tau)}\right)\right] \quad (1)$$

where

$$F_D(x) = \exp(-x^2) \int_0^x \exp(y^2) dy \quad (2)$$

In eq 1, F_D is the f-Dawson function, expressed as an integral (eq 2). The variable k_s (h^{-1}) is related to the reciprocal of time required by the product nuclei to provide complete coverage of anhydrous cement particles.^{6,25} The value of k_s depends on the product's nucleation density (I_{density} , units of μm^{-2}), that is, the number of total supercritical nuclei produced per unit surface area of cement as well as on the geometry and rate of their growth (eq 3). In the model presented in this study, the growth of the product is assumed to occur in an anisotropic fashion while varying with respect to time. $G_{\text{out}}(t)$ ($\mu\text{m}\cdot\text{h}^{-1}$) is the outward growth rate of the product, representing the direction normal to and away from the substrate (i.e., surfaces of cement particles). $G_{\text{par}}(t)$ ($\mu\text{m}\cdot\text{h}^{-1}$) is the growth rate in a lateral direction, that is, along the two-dimensional (2D) plane parallel to the boundary of the substrate. Along this 2D plane, the growth rate is assumed to be isotropic. The introduction of a time dependency on the product growth rate is a digression from the classical form of pBNG, which assumes the growth rate to remain constant throughout the hydration process. This is based on an implementation originally formulated by Bullard et al.²² and subsequently adopted by Oey et al.,³⁵ Meng et al.,¹³ and Lapeyre and Kumar⁴² to capture the temporal variation in the growth rate of C–S–H, as its supersaturation in the solution varies nonlinearly with time. As both the outward (G_{out}) and parallel (G_{par}) growth rates vary with time, a constant 2:1 ratio for $G_{\text{out}}/G_{\text{par}}$ is assumed, such that the anisotropy factor, that is, g (unitless) in eq 4, is 0.25 throughout the hydration process. This relationship between G_{out} and G_{par} represents the anisotropic growth of needlelike domains of the product^{6,25} and is in good agreement with recent experimental data of the geometry of C–S–H growth at early ages.^{26–28,30}

$$k_s = G_{\text{out}}(t) \cdot (\pi \cdot g \cdot I_{\text{density}})^{1/2} \quad (3)$$

$$g = \left(\frac{G_{\text{par}}(t)}{G_{\text{out}}(t)}\right)^2 \quad (4)$$

In eq 1, the variable k_G (h^{-1}) is related to the reciprocal of time required for the product to fill the capillary pore space. The value of k_G depends on the product's outward growth rate (G_{out}) as well as on the constant r_G (unitless), which represents the ratio of the growth rate into and out of the substrate in the normal direction (eq 5). In their study, Scherer et al.^{6,25} noted that at early ages of hydration, hydrates do not penetrate the

cement particles, and therefore, $r_G \approx 0.50$. This is because at early ages, the ionic species, that is, $\text{H}_3\text{SiO}_4^-/\text{H}_2\text{SiO}_4^{2-}$, $\text{CaOH}^+/\text{Ca}^{2+}$, and OH^- , responsible for the precipitation of C–S–H transport predominantly from the substrate's surface toward the contiguous solution while showing little movement through the product in the reverse direction.⁶ Therefore, in all simulations presented in this study, the value of r_G was assumed to be constant at 0.50. Another important parameter that dictates the value of k_G , and thus the kinetics of hydration, is the boundary area of the substrate per unit volume of the reaction vessel (a_{BV} , μm^{-1}) (eqs 5 and 6). Here, the area of the substrate is simply the initial total surface area of the cement particles. The definition of the reaction vessel, however, differs among different studies. Thomas¹² defined the reaction vessel as the space required by hydrates when the hydration of cement is complete (i.e., $\alpha = 1$), thus rendering the volume of the reaction vessel, and consequently a_{BV} , independent of the w/c ratio. As per this definition, the reaction vessel's volume is set at its minimum value, just enough to accommodate the hydrates. In several subsequent studies,^{5,6,13,25,32,35} however, the reaction vessel's volume was set at its maximum allowable value, that is, equal to the volume of the paste. On the basis of this definition, a_{BV} changes in response to changes in w/c , and the implication is that the hydrates are allowed to grow throughout the capillary pore space until either it is fully occupied or the hydration of cement is complete. As different definitions of a_{BV} exist in the literature, in this study, a modified definition has been used that allows the volume of the reaction vessel to vary between the minimum and maximum allowable values (eq 6). In eq 6, ρ is the density (water = $1000 \text{ kg}\cdot\text{m}^{-3}$ and cement = $3150 \text{ kg}\cdot\text{m}^{-3}$), and SSA_{cem} ($\text{m}^2\cdot\text{kg}^{-1}$) is the specific surface area of cement particles. The parameter p_f (unitless) acts as a free variable used in the simulations to represent the reactive paste fraction, that is, the fraction of the paste's volume within which the formation of hydrates occurs. When $p_f = 1$, the entire volume of the paste acts as the reaction vessel, whereas for fractional values of p_f , the volume of the reaction vessel is smaller than that of the paste. In such cases (i.e., $p_f < 1$), the amount of water contained within the reaction vessel is smaller than the amount of water added to the paste, though all of the solid phases (i.e., anhydrous cement particles and hydrates) are assumed to be bounded within the reaction vessel. By accounting for the excess water (i.e., water outside of the reaction vessel), the w/c ratio of the reaction vessel (w/c_{RV} , by mass) can be calculated from eq 7.

$$k_G = r_G \cdot G_{\text{out}}(t) \cdot a_{\text{BV}} \quad (5)$$

$$a_{\text{BV}} = \frac{\text{SSA}_{\text{cem}}}{\left[\frac{w/c}{\rho_{\text{water}}} + \frac{1}{\rho_{\text{cement}}}\right] \cdot p_f} \quad (6)$$

$$\frac{w}{c_{\text{RV}}} = p_f \cdot \frac{w}{c} - \left[\frac{\rho_{\text{water}}}{\rho_{\text{cement}}} \cdot (1 - p_f)\right] \quad (7)$$

The volume fraction of the product [$X(t)$], as calculated from eq 1, and the degree of hydration (α , unitless) of cement are related by a constant B (unitless)^{13,22,35} described in eq 8a

$$\alpha(t) = B \cdot X(t) \quad (8a)$$

$$B = \left[\left(\frac{\rho_{\text{cement}}}{\rho_{\text{products}}} \right) \left(c + \frac{1}{\rho_{\text{cement}}} - \frac{1}{\rho_{\text{water}}} \right) + 1 \right]^{-1} \quad (8b)$$

where, ρ_{products} is the bulk density of combined hydration products (assumed to be $2070 \text{ kg}\cdot\text{m}^{-3}$),^{43,44} and the parameter $c = -7.04 \times 10^{-5} \text{ m}^3\cdot\text{kg}^{-1}$ represents the chemical shrinkage per kilogram of cement that is consumed over the course of its hydration.⁴⁵

On the basis of the scheme described above, measured hydration rates can be simulated using the pBNG model by varying three parameters: $G_{\text{out}}(t)$, I_{density} , and p_f . Of the three parameters, I_{density} and p_f are constants with respect to time, whereas $G_{\text{out}}(t)$ varies with respect to time. Therefore, to obtain the optimum values (i.e., of I_{density} and p_f) or functional forms (i.e., of $G_{\text{out}}(t)$) of these parameters for a given system, a Nelder–Mead-based simplex algorithm^{35,46,47} that uses derivative-free and nonlinear optimization principles is employed in two steps. In the first step, the value of G_{out} is kept constant throughout the 24 h of cement hydration and fixed at $0.075 \mu\text{m}\cdot\text{h}^{-1}$ for all systems. Similar values of G_{out} have been reported in a prior study²⁶ based on scanning transmission electron microscopy (STEM) analyses of early age hydration of impure C_3S . The simplex algorithm then iteratively varies I_{density} and p_f within predefined bounds (i.e., $0.1 \mu\text{m}^{-2} \leq I_{\text{density}} \leq 1000 \mu\text{m}^{-2}$, and $0.0 \leq p_f \leq 1.0$), until the magnitude of the difference between the simulated and measured rates of product formation—expressed as $\text{d}X/\text{d}t$, or the derivative of eq 1—for each paste is minimized. It is pointed out that within the first step, the model represents the classical pBNG formulation,¹² wherein the anisotropic growth of the product nucleating at a virtual time τ (h) is kept constant throughout the hydration process. Past studies,^{13,22,35,42} however, have shown that such classical pBNG models are unable to capture the decline in the growth rate of the product as its supersaturation in the solution declines with time. Therefore, to account for the time-dependent variation in the growth rate, a second simulation step is employed. Here, at any given time t , the optimum values of I_{density} and p_f yielded from the first step are used as constants, whereas G_{out} is allowed to vary iteratively within the bounds of 10^{-4} -to- $10^2 \mu\text{m}\cdot\text{h}^{-1}$ to minimize the deviation between the simulated and measured hydration rates (expressed as $\text{d}a/\text{d}t$ or derivative of eq 8a) for each paste. When the simplex algorithm converges, the value of G_{out} is taken to be the optimum value at that time. The optimum values of G_{out} for the entire duration of cement hydration are thus determined by implementing such an optimization process over the first 24 h of hydration using a time step of 0.05 h. The time-dependent G_{out} obtained as such, mimics the growth of the product in relation to its supersaturation in the solution,^{13,22,35,42} as described in the Results and Discussion section.

RESULTS AND DISCUSSION

To study the effect of w/c on the hydration mechanisms of cement, the kinetics of hydration of two different particle size distributions (PSDs: see Figure 1) of the same cement (i.e., of the same composition) were determined. Figure 2 shows representative heat evolution profiles of pastes prepared using the coarse cement at different w/c ratios. As can be seen, despite significant differences in water contents (i.e., 58.64 and

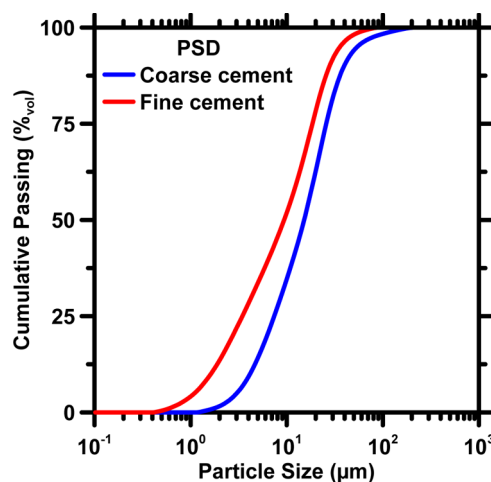


Figure 1. PSDs of the “as-received” (coarse) and ground (fine) cements measured using SLS methods. The largest uncertainty in the median diameter (d_{50} , μm) of the powders based on six replicate measurements was $\pm 6\%$.

96.93%_{vol} of water in pastes prepared at w/c of 0.45 and 10, respectively), the kinetics and degree of cement hydration within the first 24 h are broadly similar across all pastes. The lack of any significant effect of w/c was also observed for pastes prepared with the fine cement (Figure 3). These results are in good agreement with those reported in prior studies.^{12,16,31} Upon comparing the heat evolution profiles of pastes prepared with fine and coarse cements, faster hydration kinetics was noted for the former (Figure 3c). This enhancement in hydration of the fine cement is highlighted as the leftward shift of the heat evolution profile and a higher heat flow rate at the main hydration peak and can be attributed to the higher SSA of its particles,^{5,48–50} which enhances the number density of topological dissolution sites as well as sites for heterogeneous nucleation of hydrates. It should be pointed out that these enhancements in hydration rates of the fine cement are smaller in relation to the augmentation in the SSA of its particles with respect to those of the coarse cement (e.g., 72% increment in the heat flow rate at the peak vis-à-vis 125% increment in SSA). This suggests a nonlinear relationship between reactivity enhancements and surface area increments. On the basis of these results as well as those reported in prior studies,^{13,16,50} it is hypothesized that improvements in reactivity are realizable only up to a threshold level of particulate fineness. Beyond this threshold, reactivity enhancements decline due to agglomeration of the finer particles, which renders a fraction of their surface area unavailable for reaction.^{13,16,50} It is clarified, however, that the aforementioned loss in the surface area is not responsible for the apparent insensitivity to w/c .

Figures 2 and 3 qualitatively show the influence of w/c and cement fineness on the hydration kinetics of cement. To obtain quantitative information, portlandite contents of the pastes and the degree of hydration of cement after 24 h of hydration were determined using differential thermogravimetry (DTG)⁵¹ and calorimetry methods (Figure 4). As can be seen, across all w/c , portlandite contents are broadly similar, provided that the fineness of the cement does not change. Pastes prepared with the finer cement have higher portlandite contents compared to their coarser cement counterparts. This is attributed to the higher degree of hydration of the finer cement (Figure 4b). Past studies, based on microstructural investigation,^{34,52,53} have

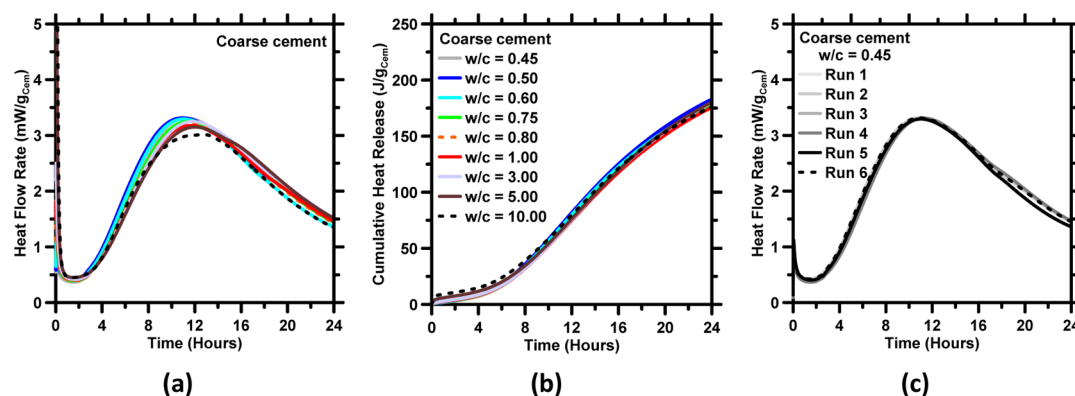


Figure 2. Isothermal microcalorimetry-based determinations of (a) heat flow rates, and (b) cumulative heat release of pastes prepared using the coarse cement at different w/c . (c) repeatability of heat flow rate determinations for a representative system. Similar analyses conducted on multiple pastes reveal that the uncertainty in the heat flow rate is within $\pm 2\%$.

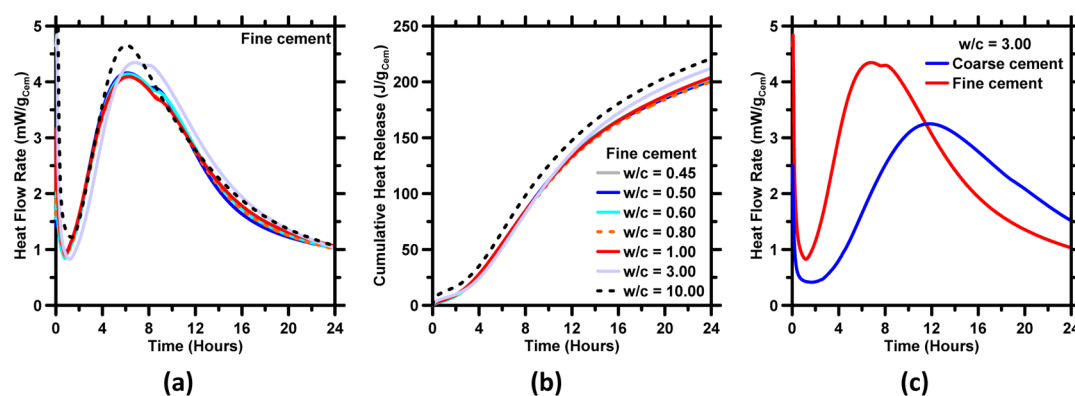


Figure 3. Isothermal microcalorimetry-based determinations of (a) heat flow rates and (b) cumulative heat release of pastes prepared using the fine cement at different w/c ratios. (c) Comparison of heat flow rates of pastes prepared at equivalent w/c using cements of different fineness.

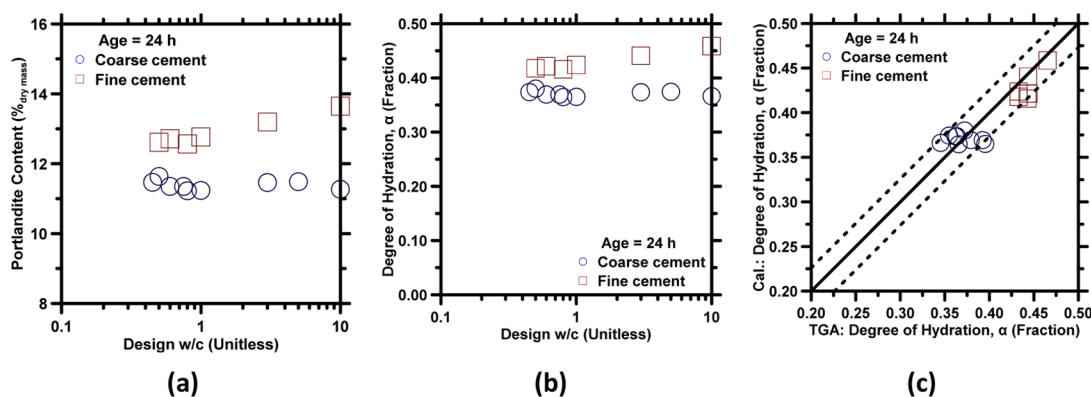


Figure 4. (a) Portlandite mass contents (as mass percent of the binder) and (b) degree of hydration of cement (α) after 24 h of hydration in pastes prepared at different w/c , as determined from DTG analyses. (c) Comparison between α calculated from microcalorimetry and DTG methods. The dashed lines represent $\pm 2.5\%$ bounds. The highest uncertainty in phase quantifications or determination of α by DTG methods is $\pm 2.5\%$.

shown that the precipitation of portlandite occurs homogeneously in the capillary pore space. This would imply that an increment in the capillary pore volume would facilitate the formation of portlandite. However, the equivalency in portlandite contents across pastes prepared at different w/c ratios suggests that the rate controlling factor for the precipitation of portlandite is not the volume of capillary pores, but rather the rate of cement hydration, which, in turn, is driven by the nucleation and growth of C–S–H.

The heat evolution profiles (Figures 2 and 3) and the results obtained from DTG analyses (Figure 4) show that the rates of

cement hydration and C–S–H precipitation are independent of the w/c and, therefore, the availability of space in the microstructural volume (i.e., capillary pore space). To quantify the evolution of the unoccupied space in the microstructure (i.e., capillary porosity) as a function of the degree of hydration of cement, the Powers model^{54,55} was used. The results obtained from the Powers model (Figure 5a) clearly show that at the degree of hydration corresponding to the time of occurrence of the main hydration peak (i.e., $\alpha = 0.13$, obtained by averaging values of α determined from calorimetry profiles of pastes prepared using the coarse cement at different w/c

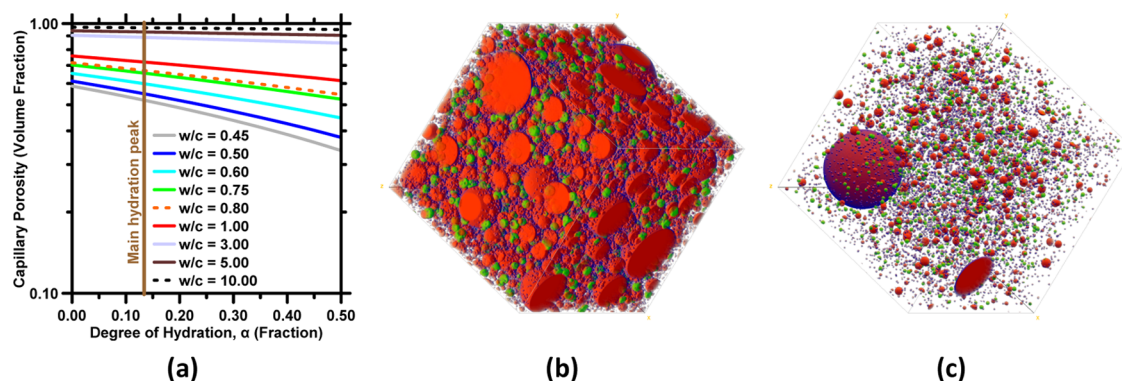


Figure 5. (a) Correlation between capillary porosity and degree of hydration (α) in pastes prepared at different w/c . In these calculations, α is provided as an input, and the corresponding capillary porosity is calculated based on the phase assemblages predicted by the Powers model.^{54,55} The solid vertical line indicates the average value of α of all pastes, prepared using the coarse cement at the main hydration peak. 3D virtual microstructures of cement pastes prepared using the coarse cement at (b) $w/c = 0.45$ and (c) $w/c = 10$ when $\alpha = 0.13$ (i.e., at the main hydration peak). The anhydrous cement particles (red) are packed as randomly dispersed spheres within the cubic representative elementary volume (size = $100 \mu\text{m}^3$). As cement reacts with water, C–S–H (blue) and other hydrates (green) are allowed to grow heterogeneously on cement surfaces and homogeneously in the pore space, respectively. See the [Supporting Information](#) (section B) for further details pertaining to the simulations.

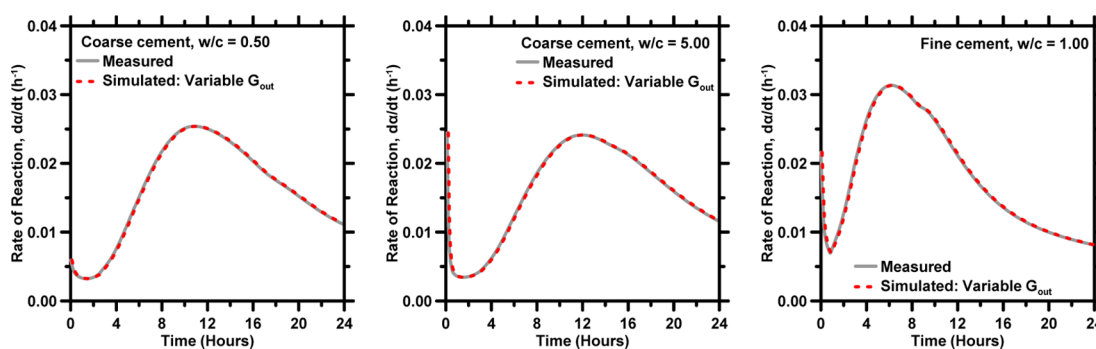


Figure 6. Representative set of simulated and measured hydration rates ($d\alpha/dt$) of cement in pastes prepared at different w/c . The red dashed line represents the final output from the simulations, wherein G_{out} is allowed to vary with time.

ratios), there is plenty of space available in the microstructural volume, even in pastes prepared at a low w/c . For example, in pastes prepared at w/c of 0.45 and 10, capillary pores comprise of 52.1 and 96.3% of the paste's volume, when $\alpha = 0.13$. The decline in the hydration rate, after the main hydration peak, in spite of the abundance in space cannot be explained solely on account of impingements between C–S–H nuclei growing on cement particle surfaces. To illustrate this point, virtual microstructures of pastes generated by a three-dimensional (3D) microstructural model^{5,16,33,42,56–59} are shown (Figure 5b,c). In these simulations, C–S–H and other hydrates (e.g., portlandite), precipitating as a result of cement hydration, are allowed to grow heterogeneously on cement particle surfaces and homogeneously in the pore space, respectively. Further details pertaining to the generation of virtual microstructures can be found in the [Supporting Information](#). As can be seen in Figure 5b,c, at the main hydration peak, although C–S–H nuclei provide partial coverage of the cement particles, impingements between C–S–H layers growing on neighboring particles are insignificant, especially in high w/c pastes. Therefore, mechanisms other than the impingements between C–S–H nuclei are responsible for deceleration of the hydration rate of cement in pastes.

To further investigate the role of w/c on cement hydration, measured hydration rates of pastes were simulated using the pBNG model. As can be seen in Figure 6, through the evaluation of optimum values of the outward growth rate of the

product ($G_{\text{out}}(t)$), the product nucleation density (I_{density}), and the reactive fraction of the paste (p_f), the model is able to reproduce the experimental results. The variations in these simulation parameters are analyzed below to describe the alterations in the nucleation and growth process in relation to the initial process parameters, that is, w/c and cement fineness.

As stated previously, within the pBNG framework, simulations are employed in two steps. In the first step, optimum values of I_{density} and p_f are determined, and in the second step, the optimum function form of $G_{\text{out}}(t)$ is determined. On the basis of the optimizations, it was found that I_{density} is $3.50 \pm 0.08 \mu\text{m}^{-2}$ for all pastes, regardless of the w/c ratio and the SSA of cement. This value of I_{density} is within the same order of magnitude of values reported in previous studies involving pBNG simulations of cement-based systems^{6,13,16,34,35} as well as those determined from STEM analyses of early age hydration of impure C_3S .²⁶ Minor differences in the values of I_{density} between this study and those derived from other pBNG models^{6,13,16,34,35} can be attributed to multiple factors including differences in the cement composition and assumptions involving the nature of growth of the product⁶ (e.g., anisotropy factor). As examples, in the simulations presented in this study, (i) changing the value of r_G from 0.5 (i.e., penetration of hydrate into the substrate grain is not permitted) to 1.0 (i.e., penetration of hydrate into the substrate is permitted) would necessitate a decrease in I_{density} ^{6,25} from ≈ 3.50 to $\approx 1.62 \mu\text{m}^{-2}$ and (ii) increasing the

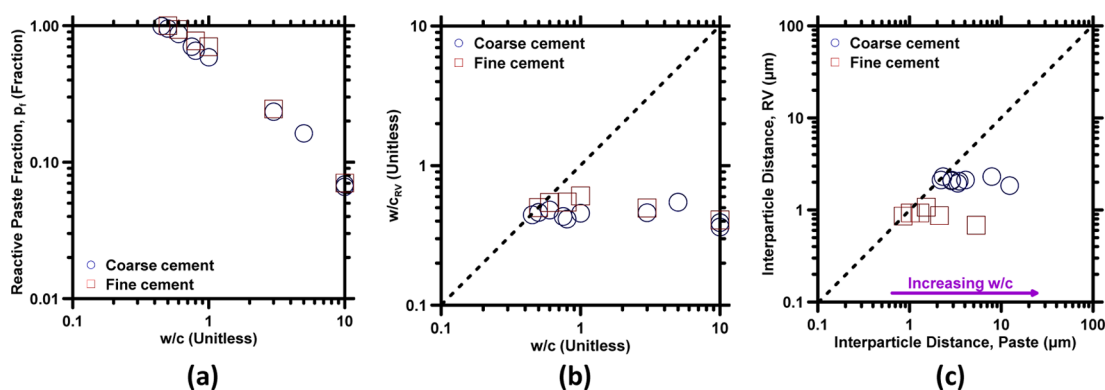


Figure 7. Parameters derived from the simulations: (a) reactive paste fraction (p_f) and (b) w/c ratio within the reaction vessel (w/c_{RV}) as functions of w/c . (c) Comparison between the average spacing between cement particle surfaces within the reaction vessel (y -axis) vis-à-vis the average spacing between them when they are assumed to remain suspended (x -axis). The dashed lines represent the lines of ideality.

anisotropy factor (g) from 0.25 to 1.0 would enhance the probability of lateral impingements between C–S–H nuclei,⁶ and, thus, require a reduction in I_{density} from ≈ 3.50 to $\approx 0.87 \mu\text{m}^{-2}$. However, regardless of the choice of these parameters, measured hydration rates of all pastes presented in this study could be fitted using a unique value of I_{density} . This equivalency in the value of I_{density} across all pastes is expected because when water is abundant, as it is during the first 24 h of hydration, the critical supersaturation at which nucleation of C–S–H occurs should be about the same and, thus, independent of the amount of water present in the system or the SSA of the cement particles.³⁵ It should be noted that at a high w/c , the larger dilution is expected to cause a slight delay in reaching C–S–H supersaturation. However, because of the intrinsically high dissolution rate of cement⁶⁰ and the very low solubility (i.e., K_{sp}) of C–S–H,^{29,44} it is expected that the solution rapidly supersaturates with respect to C–S–H in all pastes regardless of the w/c , and, thus, does not cause significant alterations (e.g., lengthening of the induction period) in the early age hydration behavior.^{26,39,61–66}

While the product nucleation density was found to be independent of the w/c , significant changes in the reactive paste fraction (p_f) were noted across different pastes (Figure 7a). As can be seen, p_f is unaffected by the cement's SSA, but decreases broadly in a linear manner with increasing w/c . This implies that as the water content of the paste increases, the formation of C–S–H is confined within smaller volume fractions of the paste. It is pointed out that if simulations are implemented by imposing a constant value of p_f (i.e., $p_f = 1$)—essentially assuming that the entire reaction vessel participates in the nucleation and growth process—the hydration rates of high w/c pastes, as estimated from the pBNG simulations, are significantly different (i.e., broader) compared to those obtained from experiments. This is because at larger values of p_f , the enlargement of the reaction vessel ensures larger spacing between the cement particles, which results in fewer impingements between product nuclei growing on neighboring particles; this manifests as a slower approach to the main hydration peak and, more importantly, a slower decline in the hydration rate after the peak. Further details pertaining to the sensitivity of the pBNG simulations with respect to variations in p_f and the justification for varying p_f are included in the Supporting Information (Figure S3).

As described previously (pBNG Model section), the reactive fraction of the paste can be described as the reaction vessel,

which consists of all of the solids (i.e., anhydrous cement particles and hydrates) but only a fraction of the capillary water. By factoring in the values of p_f (as obtained from the simulations) in eq 7, the w/c ratio within the reaction vessel (i.e., w/c_{RV}) was determined (Figure 7b). Interestingly, regardless of the w/c ratio of the paste or the SSA of cement, in all pastes, the w/c_{RV} is broadly similar, with values ranging from 0.40 to 0.51. Strikingly, these values of w/c_{RV} are in close proximity to the critical w/c (i.e., 0.42) needed for complete hydration of cement.^{54,55} This indicates that during the early stages of cement hydration, as C–S–H nucleates on cement surfaces and subsequently grows into the contiguous capillary space, its growth is confined within a region (i.e., the reaction vessel) in the vicinity of cement particles that supply the ions for C–S–H precipitation. The reaction vessel's volume is independent of the w/c and roughly equal to the critical (i.e., minimum) volume required for the occupation of the hydrates after the hydration of cement is complete (i.e., when $\alpha = 1$). Whereas the reasons for equivalency in the reaction vessel's volume across pastes prepared at different w/c ratios are not clear, it is speculated that the sedimentation of cement particles, in addition to particle-aggregation (i.e., flocculation/agglomeration caused due to interparticle forces), lead to similar particle assemblages. This definition of the reaction vessel (and, thus, of a_{BV}) is similar to that suggested by Thomas¹² and indicates that, regardless of the w/c , the calculation of a_{BV} (eq 6) for plain pastes should be based on the volume of the hydrates at $\alpha = 1$ (as the reaction vessel's volume) rather than the total volume of the paste. The results, suggesting confined growth of C–S–H on and around the cement particles, are also in good agreement with the reaction zone hypothesis advanced by Masoero et al.³⁴ In spite of similarity in findings between this study and the study by Masoero et al.,³⁴ there are differences pertaining to the origins of C–S–H's confinement, which are highlighted below.

In the model used by Masoero et al.,³⁴ it is assumed that the cement particles remain suspended, and the growth of C–S–H occurs in a confined region (i.e., in the semipore space) in proximity to the cement particles. First, in practice, because of the large density difference between cement (i.e., $3150 \text{ kg}\cdot\text{m}^{-3}$) and water (i.e., $1000 \text{ kg}\cdot\text{m}^{-3}$), the sedimentation of cement particles always occurs in pastes (in the absence of viscosity-modifying admixtures or when in situ mixing is not employed), as was also observed in the current experiments. Second, the assumption of particles being suspended combined with the

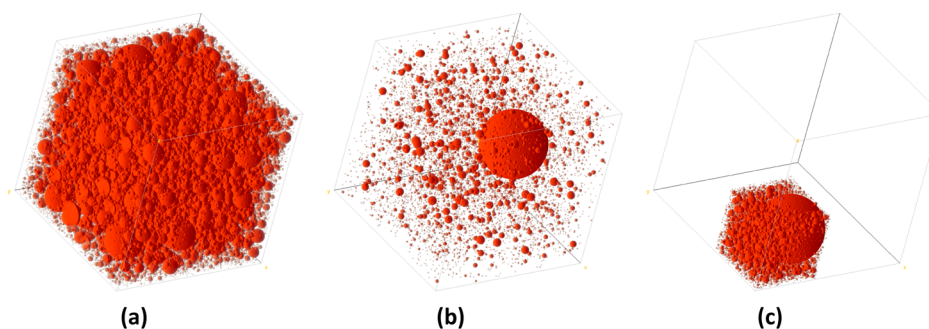


Figure 8. 3D virtual microstructures showing the packing of particles at the time of mixing (i.e., without sedimentation of particles) in pastes prepared at (a) $w/c = 0.45$ and (b) $w/c = 10$. (c) effects of sedimentation of particles in a paste prepared at $w/c = 10$. The smaller cubic volume schematically represents the reaction vessel, which includes all of the cement particles but only a fraction of the water. The volumetric content of water in the reaction vessel is derived from w/c_{RV} , as calculated from pBNG simulations.

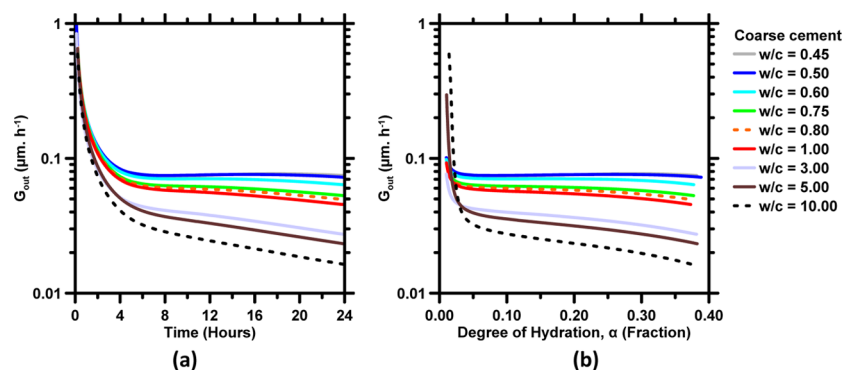


Figure 9. Outward growth rate of the product (G_{out}) as a function of the (a) time and (b) degree of hydration of the coarse cement.

confinement of C–S–H, as assumed in the model developed by Masoero et al.,³⁴ significantly marginalizes the likelihood of impingement between C–S–H layers growing on different particles, especially at early ages when the degree of hydration of cement is low. This is difficult to reconcile as the setting of the paste,⁶⁷ which occurs at a low degree of hydration of cement, necessitates such early age impingements between C–S–H layers growing on adjacent cement grains. In contrast to the model presented in ref 34, the pBNG model used in this study does not incorporate any assumption regarding the occurrence, or lack thereof, of sedimentation of cement particles. However, based on the simulation results, which indicate that in high w/c pastes, the reaction vessel is consistently smaller than the paste's volume (Figure 7), it is inferred that the sedimentation of cement particles does occur. This inference gains support from experiments, in which the solids (i.e., cement particles and hydrates) were consistently found to be settled at the bottom of the reaction container after 24 h of hydration. This assemblage of cement particles within a fraction of the paste's volume causes the particles to pack more closely as compared to an equivalent system in which particles remain suspended.

To better illustrate the effects of sedimentation of cement particles on particle packing, the 3D microstructural model, described above and in ref^{8,16,33,56–59} was used to generate virtual microstructures for two cases: one in which cement particles remain suspended and the other in which sedimentation occurs. In the former and latter cases, the water contents resemble the original w/c and the w/c_{RV} (determined from pBNG simulations), respectively. Once the sought packing is achieved, the average initial spacing between cement particle surfaces (i.e., interparticle distance) is

calculated using algorithms described in ref 68. The virtual microstructures generated from the simulations are shown in Figure 8, and the calculated interparticle distances are shown in Figure 7c. As can be seen, because of the sedimentation of cement particles in high w/c pastes, the interparticle distance within the reaction vessel is reduced to a fraction of the interparticle distance at the time of mixing (i.e., when sedimentation has not occurred). It is also noteworthy that across pastes prepared using the same PSD of cement but at different w/c ratios, the interparticle distances within the reaction vessel remain broadly the same. This is due to the equivalency in the values of w/c_{RV} (Figure 7b) and suggests that as cement particles settle, their assemblage and access to water needed for hydration remain broadly the same regardless of the original w/c . In pastes prepared with the fine cement, the interparticle distances within the reaction vessel are smaller (i.e., $\approx 1.0 \mu\text{m}$) as compared to those prepared with the coarse cement (i.e., $\approx 2.1 \mu\text{m}$), although the volumes of the reaction vessel are equivalent across all pastes. This is attributed to the larger number of particles (per unit mass) in the fine cement. These interparticle distances, presented in Figure 7c, are analogous to the size of the reaction zone reported by Masoero et al.,³⁴ as in both studies, these sizes represent the linearized space within which the growth of C–S–H occurs and remains confined. In this study, the interparticle distances range between 1.0 and 2.1 μm , whereas in ref 34, the sizes of the reaction zone were estimated between ≈ 0.38 and $\approx 1.1 \mu\text{m}$. It is reasonable to say that these differences are small and can be attributed to differences in the schemes (e.g., anisotropy in the growth of C–S–H) employed in the pBNG simulations as well as the differences in the properties (i.e., PSD and composition) of the cementing material. The assumption of particles

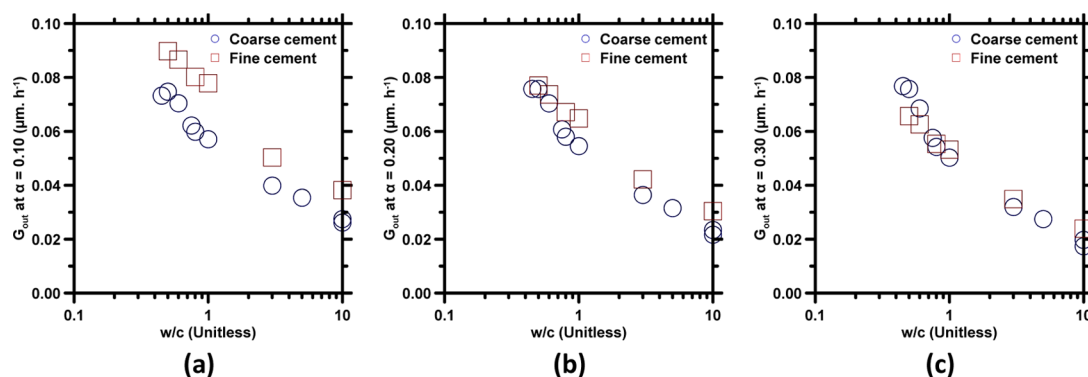


Figure 10. Outward growth rate of the product (G_{out}) as a function of w/c when (a) $\alpha = 0.10$, (b) $\alpha = 0.20$, and (c) $\alpha = 0.30$. Results for both coarse and fine cements are shown.

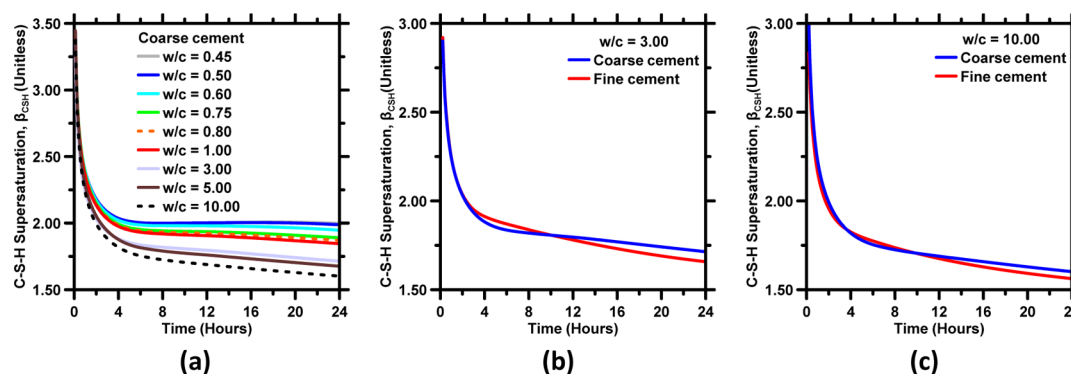


Figure 11. Estimated temporal evolution of the supersaturation of C-S-H (β_{CSH}) in pastes prepared using (a) the coarse cement at different w/c , (b) the coarse and fine cements at $w/c = 3$, and (c) the coarse and fine cements at $w/c = 10$.

remaining suspended, as implemented in ref 34, is also expected to alter the likelihood of impingement between C-S-H nuclei and, thus, contribute to the aforementioned differences.

On the basis of these results, it is hypothesized that the confinement of C-S-H is a manifestation of the space constraint induced by the close packing of the settled cement particles within the reaction vessel. Because of the smaller spacing between cement particles within the reaction vessel, C-S-H layers growing on adjacent cement particles are able to percolate and cause the paste to set, even when the w/c is relatively high (e.g., $w/c = 0.75$). The enhanced impingements between C-S-H layers as well as the impingements between C-S-H nuclei growing on the same particle contribute toward the occurrence of the main hydration peak, which occurs within 12 h of hydration and at a low degree of hydration (i.e., $\alpha \approx 0.13$) even in pastes prepared at high w/c (Figures 2 and 3). In addition to these impingements, the temporal variation in the growth rate of C-S-H (described below), as driven by its supersaturation, is expected to affect the hydration rates.

Figure 9a describes the influence of w/c on the product growth rate [$G_{out}(t)$]. As shown, the product grows at rates that decrease nonlinearly by about 2 orders of magnitude over the course of cement hydration in the first 24 h. This functional form of the growth rate has been reported^{13,22,35} to mimic the evolving supersaturation of C-S-H in the solution, wherein high and low supersaturations imply larger and smaller driving forces for C-S-H growth, respectively. It is noted that at any given time (Figure 9a) or degree of hydration of cement (Figure 9b), G_{out} decreases with increasing w/c . This is better shown in Figure 10, which plots the growth rates of pastes, extracted at $\alpha = 10$, 20, and 30% against the w/c . The

diminishment of the product growth rate with increasing w/c suggests abatement in the driving force for C-S-H growth in diluted systems. It is hypothesized that in high w/c systems, though C-S-H is confined within a smaller fraction of the paste volume (i.e., the reaction vessel), the ions²⁹ (i.e., $\text{H}_3\text{SiO}_4^-/\text{H}_2\text{SiO}_4^{2-}$, $\text{CaOH}^+/\text{Ca}^{2+}$, and OH^-) responsible for the precipitation of C-S-H are able to transport across the entire paste's volume. As such, the supersaturation of C-S-H in the solution and, hence, the driving force for its growth are sensitive to the paste's water content and decrease with increasing w/c ; this point is described in more detail through experimental results further in the text. This decrease in C-S-H supersaturation manifests as a systematic diminishment of its growth rate with increasing w/c (Figures 9 and 10). It is pointed out that, in spite of the ions being able to move throughout the paste's volume, it is expected that their abundance is relatively higher in regions in proximity to their source, that is, cement particles. This would imply higher supersaturation and, therefore, higher growth rate of C-S-H around the cement particles. While the current simulations do not consider gradients in ion concentrations, results shown in Figure 10 do support the theory. As can be seen, at equivalent w/c , growth rates at early ages (i.e., when $\alpha = 0.10$) are higher in pastes prepared with the fine cement as compared to those prepared with the coarse cement. This is hypothesized to be on account of smaller spacing between particles (Figure 7c) in pastes prepared with the fine cement, such that the overlapping (or closely packed) ion-abundant regions around the closely packed particles bolster the driving force for the growth of C-S-H. At later ages, when the supersaturation of C-S-H in the solution is low,²² the effect of interparticle spacing on the

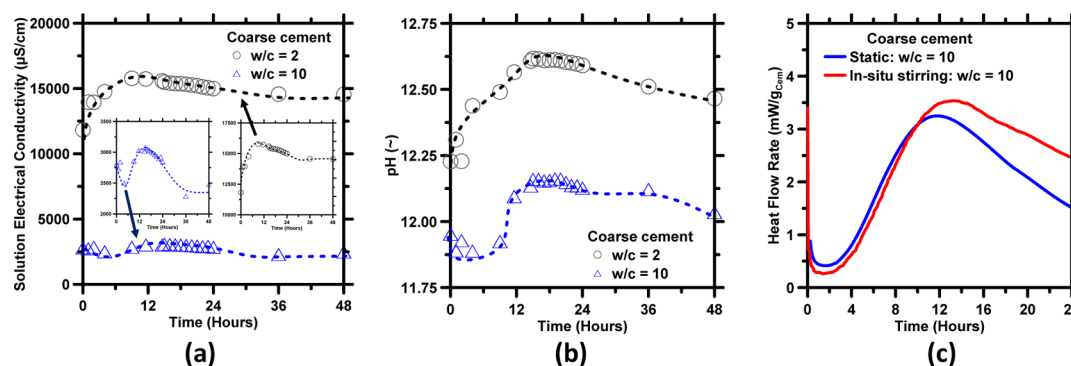


Figure 12. (a) Electrical conductivity and (b) pH of the pore solution of pastes prepared using the coarse cement at different w/c . Because of the large difference in the magnitudes of the solution's electrical conductivity, rescaled subplots for the two curves are included within (a). (c) Heat flow rates of pastes, prepared using the coarse cement at $w/c = 10$, measured without (static) and with in situ stirring.

growth rate diminishes. This is reflected in Figure 10b,c, which show that at higher degrees of cement hydration, growth rates are independent of the spacing between particles (or fineness of the cement).

The growth rates shown in Figure 9 qualitatively allude to the temporal evolution of the supersaturation of C–S–H in the solution. For quantitative determinations of the supersaturation, a generic relationship between the growth rate and supersaturation of C–S–H must be known. In a recent study, Scherer et al.²⁷ showed that the growth rate of C–S–H exhibits a cubic dependence on its supersaturation, as shown in eq 9.

$$G_{\text{out}}(t) = G_{\text{out-c}} [\beta_{\text{CSH}}(t) - 1]^3 \quad (9)$$

where, $G_{\text{out-c}}$ ($\mu\text{m h}^{-1}$) is a constant and $\beta_{\text{CSH}}(t)$ (unitless) is the time-dependent supersaturation of C–S–H in the solution. As the exact value of $G_{\text{out-c}}$ is not known and is expected to change depending on the concentration of calcium (i.e., Ca^{2+}) in the solution,²⁷ a value of $G_{\text{out-c}} = 0.075 \mu\text{m h}^{-1}$ is assumed in this study. This value, as described previously, is used in the first step of the pBNG simulations and is within the same order of magnitude as experimental values.^{26,27,64} By plugging in the estimated value of $G_{\text{out-c}}$ and $G_{\text{out}}(t)$ (i.e., obtained from pBNG simulations) in eq 9, the temporal evolution of β_{CSH} in the pastes was estimated (Figure 11). Admittedly, on account of the uncertainty in the values of $G_{\text{out-c}}$, the values of β_{CSH} are expected to be a rough, rather than an accurate estimate. However, these estimated values are expected to capture the effects of variations in the process parameters, that is, w/c and SSA of cement, as they are all derived using the same value of $G_{\text{out-c}}$.

The temporal evolutions of β_{CSH} , shown in Figure 11, are qualitatively similar to those reported in the literature and derived from kinetic cellular automata simulations^{22,27,29,30,61,69} and reflect the trends in the abundance of aqueous ionic species—the silicate species (i.e., $\text{H}_2\text{SiO}_4^{2-}$ and H_3SiO_4^-) in particular—in the solution.^{61,69–72} At very early ages (i.e., around the time of mixing), when C–S–H is present in small amounts and cement continues to dissolve rapidly releasing ions at a fast rate into the solution, β_{CSH} is expectedly high. With time, the dissolution rate of cement declines, and more ions, including aqueous silicate species, are consumed as the rate of precipitation of C–S–H increases; this manifests as a steep decline in β_{CSH} . It should be noted, however, that this decline in β_{CSH} is nonmonotonic, particularly in the case of low w/c systems. Specifically, around the main hydration peak, β_{CSH} increases—albeit slightly—and then continues to decrease.

These minor fluctuations in the evolution of β_{CSH} are expected to mimic the increase in the silicate concentration that occurs around the main hydration peak when there is a sharp decrease in the Ca^{2+} concentration.^{22,35} At later ages (i.e., in the subsequent hours following the main hydration peak), ion concentrations in the solution stabilize,^{22,39,61,70} and thus β_{CSH} also stabilizes. At any given time, pastes prepared at a lower w/c have higher β_{CSH} as compared to those prepared at a higher w/c . This, as stated previously, is expected to be due to the larger dilution in the higher w/c pastes and is corroborated by the evolutions of the solution electrical conductivity and pH. As can be seen in Figure 12a,b, whereas the overall profiles of electrical conductivity and pH evolution are similar across different w/c —which is expected due to similar hydration kinetics (Figure 2)—the magnitudes of both parameters at equivalent times are lower in high w/c pastes on account of higher dilution (i.e., larger volume of solution per mole of a given ion). Lower concentration of ions in the pore solutions of high w/c pastes causes β_{CSH} to be lower compared to those prepared at low w/c . It is also interesting to note that β_{CSH} is broadly insensitive to the PSD of cement (Figure 11b,c). This suggests that the differences in the hydration kinetics induced by the SSA of cement (as shown in Figure 3) are unable to cast a significant impact on the composition of the solution and, therefore, the supersaturation of C–S–H.

Overall, the results described thus far suggest that the hydration kinetics of cement is not affected by the w/c on account of the sedimentation of cement particles. As cement particles settle, they are packed more closely, which in turn creates a space constraint for the growth of C–S–H and results in its confinement. On the basis of this theory, it could be hypothesized that if the sedimentation of cement particles is prevented—or even disrupted—C–S–H would not remain confined, thus causing the hydration kinetics to change. To test this hypothesis, hydration kinetics was monitored for a paste prepared at $w/c = 10$, wherein the paste was continuously stirred at a low speed (i.e., 80 rpm) using an electrically-driven agitator throughout the 24 h of hydration. It is clarified that the low rotational speed of the agitator minimizes the heat released due to mixing action (i.e., $<0.15 \text{ J}$ of cumulative heat over a 24 h period, see the Supporting Information) but is unable to completely prevent the sedimentation of cement particles. As shown in Figure 12c, in the stirred paste, the hydration rates are indeed different—broader, with delayed occurrence of the main hydration peak and slower postpeak decline of the hydrate rate—compared to the static paste (i.e., without in situ mixing).

These differences can be reconciled by considering the effect of stirring on the spacing between cement particles. Specifically, in the stirred pastes, sedimentation of cement particles is partially prevented, which results in larger spacing between them and, consequently, fewer impingements between C–S–H layers growing on neighboring cement particles. Because of such lack in confinement of C–S–H in the stirred pastes, the main hydration peak is delayed and the decline in the postpeak hydration rate is slower. By contrast, in the static paste, the closely packed cement particles ensure more impingements between the C–S–H layers and thus a faster approach to and departure from the main hydration peak. The results shown in Figure 12 are in good agreement with the results shown in Figure S3b (of the Supporting Information), wherein it is shown that if the reaction vessel's volume is larger (i.e., $p_f \approx 1.00$), the pBNG-simulated hydration rates of high w/c pastes have a delayed occurrence of the main hydration peak and a slower postpeak decline of the hydration rate. The results shown in Figure 12 are also in good agreement with a prior study,³¹ which shows that in pastes provisioned with dispersants, the enhanced dispersion of cement particles causes cement hydration rates to change (i.e., to get progressively broader) in relation to increasing w/c .

On the basis of these results, it is hypothesized that sedimentation of cement particles is at the origin of C–S–H confinement and insensitivity of cement hydration rates to changes in w/c . It is clarified that, although this hypothesis has been construed from the hydration behavior of water-rich systems (i.e., $w/c > 0.42$), past studies^{12,31} and additional data included in the Supporting Information show that early age hydration rates of low w/c pastes (i.e., $w/c < 0.42$) are also insensitive to w/c . Results obtained from pBNG simulations (not shown) indicate that even in low w/c pastes, the reaction vessel's volume is equivalent to the volume occupied by hydrates at $\alpha = 1$. Thus, it is proposed that in pBNG models, to account for C–S–H confinement, the determination of the boundary area per unit volume of the substrate (a_{BV} : eq 6) for plain pastes should be calculated based on the volume of hydrates that would form when all of the cement has reacted, rather than the total volume of the paste (including excess water) which depends on the w/c . As per this definition, in blended systems wherein cement is partially replaced by a filler, a_{BV} would be equal to the ratio of the total solid surface area at $\alpha = 0$ (i.e., combined surface areas of cement and filler) to the total volume of solids at $\alpha = 1$ (i.e., combined volumes of hydrates and filler). As pointed out by Scherer and Bellmann,²⁷ pBNG models should account for the highly nonlinear supersaturation-dependent variation in the growth rate of C–S–H. In this study, although the evolution of growth rate and supersaturation of C–S–H were derived indirectly from heat evolution profiles, it is possible to incorporate a supersaturation-dependent growth rate directly into pBNG models through experimental measurements of the evolving solution composition.²⁷ Last, it is recognized that further investigation of cement hydration kinetics in pastes, wherein sedimentation of particles is progressively mitigated (e.g., using viscosity-modifying admixtures), is required for validation and further refinement of the hypotheses presented in this study. A study focused on the description of hydration kinetics of C_3S suspensions, with and without the disruption of particle sedimentation, is currently underway at Missouri S&T; outcomes of this study will be presented in a future publication.

CONCLUSIONS

A series of experiments and pBNG simulations were applied to elucidate the role of w/c ratio on the hydration kinetics of cement in plain pastes. The experiments, conducted using isothermal microcalorimetry methods, show that cement hydration rates are insensitive to changes in w/c . As classical pBNG models are unable to explain such effects, a modified pBNG model is presented, in which the growth of the main hydrate, that is, C–S–H, is assumed to be anisotropic and allowed to vary in relation to the nonlinear evolution of its supersaturation in the solution.

Results obtained from the pBNG simulations show that the nucleation density of C–S–H, forming heterogeneously on cement surfaces, is unaffected by the w/c of the paste as well as the SSA of cement particulates. However, as the w/c increases, the fraction of the paste's volume that participates in the nucleation and growth process reduces. This reactive (i.e., participatory) fraction of the paste, termed as the reaction vessel in this study, was found to be equivalent (i.e., equivalent size/volume and water content) across pastes prepared at different w/c ratios and cements of different SSAs.

On the basis of these results, it is hypothesized that at early ages, the nucleation and growth of C–S–H remains confined within the reaction vessel, such that its formation is limited to ion-abundant regions in proximity to cement particles. This confinement of C–S–H is hypothesized to be a manifestation of the sedimentation of cement particles. As cement particles settle, they are packed more closely, which in turn creates a space constraint for the growth of C–S–H and results in its confinement. Indeed, in pastes, wherein the sedimentation of cement particles is disrupted using in situ stirring, the hydration kinetics is no longer insensitive to changes in the w/c .

Results from this study also suggest that, unlike C–S–H, the ions in solution are not confined within the reaction vessel. The transport of ions throughout the volume of the paste causes the supersaturation of C–S–H, that is, the driving force for its growth, to decline with increasing w/c . This results in a systematic diminishment of C–S–H growth rate with increasing w/c .

Overall, the outcomes of this work provide novel insights into the mechanisms that cause cement hydration rates to remain insensitive to changes in the paste's water content. Whereas a simplified view is presented, the discussion highlights important aspects that need to be incorporated in pBNG models to account for C–S–H confinement as well as the sedimentation of cement particles. Investigation of the cement hydration kinetics in systems, wherein sedimentation of particles is progressively mitigated (e.g., using viscosity modifying admixtures), is expected to aid in validation and in further refinement of the hypotheses presented in this study.

MATERIALS AND METHODS

A commercially available type I ordinary portland cement with an estimated crystalline phase composition of 61% C_3S , 8% C_2S , 6% C_3A , 9% C_4AF , and 3.4% of gypsum ($CaSO_4 \cdot 2H_2O$) was used in this study. Further details pertaining to the chemical composition of cement—as obtained using a combination of X-ray fluorescence and quantitative X-ray diffraction (XRD) methods—are provided in the Supporting Information. The cement, as received from the supplier, was ground using a ring grinder to generate two different PSDs. In the subsequent discussions, the “as-received” and ground

cements are referred to as coarse and fine cements, respectively. The PSDs of the cements, shown in Figure 1, were measured using a Beckman Coulter static light scattering (SLS) analyzer (LS13-320) using a 750 nm laser source that is incident on a dilute suspension of powder particles in isopropyl alcohol, dispersed by ultrasonication. The median particle sizes (d_{50} , μm) of the PSDs of the coarse and fine cements were determined as 15.55 and 9.23 μm , respectively. By factoring the bulk density (i.e., 3150 $\text{kg}\cdot\text{m}^{-3}$, as measured using a pycnometer), the total SSA ($\text{m}^2\cdot\text{kg}^{-1}$) of the coarse and fine cements were calculated from the PSDs as 196 and 441 $\text{m}^2\cdot\text{kg}^{-1}$, respectively. XRD patterns were obtained for the coarse and fine cements, and based on the results, it was confirmed that there was no change in the cement's composition as a result of the grinding.

To study the effects of the water content, cement + water mixtures were prepared at different w/c (mass basis) ranging from 0.45 to 10. Low and high w/c cementitious mixtures are typically described as paste and suspension, respectively. However, as the limiting w/c beyond which a mixture ceases to be a paste (or becomes a suspension) is not well-known, in this paper, all mixtures are referred to as pastes. It should be noted that all pastes included in this study are water-rich, as their w/c exceeds the critical value of 0.42 (i.e., minimum w/c needed for complete hydration of cement).^{54,55}

The rate and extent of hydration were monitored up to 24 h after mixing using a TAM IV isothermal conduction microcalorimeter programmed to maintain the sample at a constant temperature of 20 ± 0.1 $^{\circ}\text{C}$. Compared to conventional methods of reactivity assessment (e.g., isothermal calorimetry), microcalorimetry methods are considered more accurate as they allow quantification of the heat flow rate of the reaction at a very high resolution (10^{-7} J/s), which enables monitoring the dissolution of compounds even at high dilutions.^{13,73,74} The titration cell (maximum diameter = 1.25 cm) of the microcalorimeter is fitted with an electrically driven agitator, which allows in situ mixing of hydrating pastes prepared at high w/c . However, with the exception of selected experiments (which are identified in the text), heat evolution profiles of all pastes discussed in this paper were obtained without the use of the agitator. In situ mixing was purposely avoided for two reasons: (i) to mimic practical concrete mixing protocols, which are also devoid of in situ mixing and (ii) to maintain consistent protocols across experiments, as in situ mixing cannot be applied to low w/c pastes. The cumulative and differential heat release obtained from calorimetry experiments were normalized by the enthalpy of cement hydration (as calculated from mass fractions and enthalpy of individual phases⁵), 472 J $\cdot \text{g}_{\text{cement}}^{-1}$, to determine the extent of hydration^{13,16} (i.e., degree of hydration, α , expressed as the fraction of cement reacted) and the rate of hydration (i.e., $d\alpha/dt$, h^{-1}) of cement, respectively, as functions of time. This method of derivation of α and $d\alpha/dt$ is based on the assumption that the measured heat release is solely on account of cement hydration. In addition to monitoring the evolution of heat linked to hydration, the evolutions of the electrical conductivity and pH of the pore solution of the pastes were measured at discrete time steps between mixing and 48 h of hydration. These measurements were carried out using a HI5522 electric conductivity and pH meter with the HI76312 and HI1131 probes, respectively. Samples used for these measurements were prepared using the same protocols as those for calorimetry experiments.

A Netzsch STA 409 PC thermogravimetric analyzer was used to identify and measure the quantities of phases present at different hydration times. Toward this, the mass loss (thermogravimetry) and the differential mass loss (DTG) traces were processed to quantify the degree of hydration and phase contents, that is, loss on ignition, evaporable and nonevaporable water, portlandite, and calcite (if any may have formed because of carbonation of calcium-rich phases). For these quantifications (i.e., α and phase contents), well-established methods detailed in prior studies^{51,75} were used.

■ ASSOCIATED CONTENT

Supporting Information

The Supporting Information is available free of charge on the ACS Publications website at DOI: 10.1021/acsomega.8b00097.

Cement composition and mixing procedure, description of the 3D microstructural model, description of the isothermal microcalorimetry method, sensitivity of pBNG parameters, and heat evolution profiles of water-deficient pastes (PDF)

■ AUTHOR INFORMATION

Corresponding Author

*E-mail: kumarad@mst.edu. Phone: 573-341-6994 (A.K.).

ORCID

Aditya Kumar: 0000-0001-7550-8034

Notes

The authors declare no competing financial interest.

■ ACKNOWLEDGMENTS

This research was conducted in the Materials Research Center (MRC) at Missouri S&T. The authors gratefully acknowledge the financial support that has made these laboratories and their operations possible. Funding for this research was provided by the National Science Foundation [NSF, CMMI: 1661609], MRC at Missouri S&T [MRC Young Investigator Seed Funding] and the University of Missouri Research Board [UMRB].

■ REFERENCES

- (1) Bullard, J. W.; Jennings, H. M.; Livingston, R. A.; Nonat, A.; Scherer, G. W.; Schweitzer, J. S.; Scrivener, K. L.; Thomas, J. J. Mechanisms of Cement Hydration. *Cem. Concr. Res.* **2011**, *41*, 1208–1223.
- (2) Scrivener, K. L.; Juilland, P.; Monteiro, P. J. M. Advances in Understanding Hydration of Portland Cement. *Cem. Concr. Res.* **2015**, *78*, 38–56.
- (3) Taylor, H. F. W. *Cement Chemistry*, 2nd ed.; Thomas Telford: London, United Kingdom, 1997.
- (4) Thomas, J. J.; Biernacki, J. J.; Bullard, J. W.; Bishnoi, S.; Dolado, J. S.; Scherer, G. W.; Luttge, A. Modeling and Simulation of Cement Hydration Kinetics and Microstructure Development. *Cem. Concr. Res.* **2011**, *41*, 1257–1278.
- (5) Kumar, A.; Bishnoi, S.; Scrivener, K. L. Modelling Early Age Hydration Kinetics of Alite. *Cem. Concr. Res.* **2012**, *42*, 903–918.
- (6) Scherer, G. W.; Zhang, J.; Thomas, J. J. Nucleation and Growth Models for Hydration of Cement. *Cem. Concr. Res.* **2012**, *42*, 982–993.
- (7) Avrami, M. Kinetics of Phase Change. I General Theory. *J. Chem. Phys.* **1939**, *7*, 1103–1112.
- (8) Avrami, M. Granulation, Phase Change, and Microstructure Kinetics of Phase Change. III. *J. Chem. Phys.* **1941**, *9*, 177–184.
- (9) Jun, S.; Zhang, H.; Bechhoefer, J. Nucleation and Growth in One Dimension. I. The Generalized Kolmogorov-Johnson-Mehl-Avrami

Model. *Phys. Rev. E: Stat., Nonlinear, Soft Matter Phys.* **2005**, *71*, 011908.

(10) Cahn, J. W. The Kinetics of Grain Boundary Nucleated Reactions. *Acta Metall.* **1956**, *4*, 449–459.

(11) Thomas, J. J.; Jennings, H. M.; Chen, J. J. Influence of Nucleation Seeding on the Hydration Mechanisms of Tricalcium Silicate and Cement. *J. Phys. Chem. C* **2009**, *113*, 4327–4334.

(12) Thomas, J. J. A New Approach to Modeling the Nucleation and Growth Kinetics of Tricalcium Silicate Hydration. *J. Am. Ceram. Soc.* **2007**, *90*, 3282–3288.

(13) Meng, W.; Lunkad, P.; Kumar, A.; Khayat, K. Influence of Silica Fume and Polycarboxylate Ether Dispersant on Hydration Mechanisms of Cement. *J. Phys. Chem. C* **2016**, *120*, 26814–26823.

(14) Nicoleau, L.; Nonat, A.; Perrey, D. The Di- and Tricalcium Silicate Dissolutions. *Cem. Concr. Res.* **2013**, *47*, 14–30.

(15) Nicoleau, L.; Bertolim, M. A. Analytical Model for the Alite (C3S) Dissolution Topography. *J. Am. Ceram. Soc.* **2016**, *99*, 773–786.

(16) Oey, T.; Kumar, A.; Bullard, J. W.; Neithalath, N.; Sant, G. The Filler Effect: The Influence of Filler Content and Surface Area on Cementitious Reaction Rates. *J. Am. Ceram. Soc.* **2013**, *96*, 1978–1990.

(17) Masoero, E.; Del Gado, E.; Pellenq, R. J.-M.; Ulm, F.-J.; Yip, S. Nanostructure and Nanomechanics of Cement: Polydisperse Colloidal Packing. *Phys. Rev. Lett.* **2012**, *109*, 155503.

(18) Price, C. W. Use of Kolmogorov-Johnson-Mehl-Avrami Kinetics in Recrystallization of Metals and Crystallization of Metallic Glasses. *Acta Metall. Mater.* **1990**, *38*, 727–738.

(19) Kolmogorov, A. N. On the Statistical Theory of the Crystallization of Metals. *Bull. Acad. Sci. USSR, Math. Ser.* **1937**, *1*, 355–359.

(20) Peterson, V. K.; Whitten, A. E. Hydration Processes in Tricalcium Silicate: Application of the Boundary Nucleation Model to Quasielastic Neutron Scattering Data. *J. Phys. Chem. C* **2009**, *113*, 2347–2351.

(21) Peterson, V. K.; Juenger, M. C. G. Hydration of Tricalcium Silicate: Effects of CaCl₂ and Sucrose on Reaction Kinetics and Product Formation. *Chem. Mater.* **2006**, *18*, 5798–5804.

(22) Bullard, J. W.; Scherer, G. W.; Thomas, J. J. Time Dependent Driving Forces and the Kinetics of Tricalcium Silicate Hydration. *Cem. Concr. Res.* **2015**, *74*, 26–34.

(23) Valentini, L.; Favero, M.; Dalconi, M. C.; Russo, V.; Ferrari, G.; Artioli, G. Kinetic Model of Calcium-Silicate Hydrate Nucleation and Growth in the Presence of PCE Superplasticizers. *Cryst. Growth Des.* **2016**, *16*, 646–654.

(24) Ridi, F.; Fratini, E.; Luciani, P.; Winnefeld, F.; Baglioni, P. Tricalcium Silicate Hydration Reaction in the Presence of Comb-Shaped Superplasticizers: Boundary Nucleation and Growth Model Applied to Polymer-Modified Pastes. *J. Phys. Chem. C* **2012**, *116*, 10887–10895.

(25) Scherer, G. W. Models of Confined Growth. *Cem. Concr. Res.* **2012**, *42*, 1252–1260.

(26) Bazzoni, A.; Ma, S.; Wang, Q.; Shen, X.; Cantoni, M.; Scrivener, K. L. The Effect of Magnesium and Zinc Ions on the Hydration Kinetics of C3S. *J. Am. Ceram. Soc.* **2014**, *97*, 3684–3693.

(27) Scherer, G. W.; Bellmann, F. Kinetic Analysis of C-S-H Growth on Calcite. *Cem. Concr. Res.* **2018**, *103*, 226–235.

(28) Zhang, Z.; Scherer, G. W.; Bauer, A. Morphology of Cementitious Material during Early Hydration. *Cem. Concr. Res.* **2018**, *107*, 85–100.

(29) Bullard, J. W.; Scherer, G. W. An Ideal Solid Solution Model for C-S-H. *J. Am. Ceram. Soc.* **2016**, *99*, 4137–4145.

(30) Bellmann, F.; Scherer, G. W. Analysis of C-S-H Growth Rates in Supersaturated Conditions. *Cem. Concr. Res.* **2018**, *103*, 236–244.

(31) Kirby, D. M.; Biernacki, J. J. The Effect of Water-to-Cement Ratio on the Hydration Kinetics of Tricalcium Silicate Cements: Testing the Two-Step Hydration Hypothesis. *Cem. Concr. Res.* **2012**, *42*, 1147–1156.

(32) Oey, T.; Stoian, J.; Li, J.; Vong, C.; Balonis, M.; Kumar, A.; Franke, W.; Sant, G. Comparison of Ca(NO₃)₂ and CaCl₂ Admixtures on Reaction, Setting, and Strength Evolutions in Plain

and Blended Cementing Formulations. *J. Mater. Civ. Eng.* **2014**, *27*, 04014267.

(33) Kumar, A.; Sant, G.; Patapy, C.; Gianocca, C.; Scrivener, K. L. The Influence of Sodium and Potassium Hydroxide on Alite Hydration: Experiments and Simulations. *Cem. Concr. Res.* **2012**, *42*, 1513–1523.

(34) Masoero, E.; Thomas, J. J.; Jennings, H. M. A Reaction Zone Hypothesis for the Effects of Particle Size and Water-to-Cement Ratio on the Early Hydration Kinetics of C3S. *J. Am. Ceram. Soc.* **2014**, *97*, 967–975.

(35) Oey, T.; Kumar, A.; Falzone, G.; Huang, J.; Kennison, S.; Bauchy, M.; Neithalath, N.; Bullard, J. W.; Sant, G. The Influence of Water Activity on the Hydration Rate of Tricalcium Silicate. *J. Am. Ceram. Soc.* **2016**, *99*, 2481–2492.

(36) Quennoz, A.; Scrivener, K. L. Hydration of C3A–gypsum Systems. *Cem. Concr. Res.* **2012**, *42*, 1032–1041.

(37) Minard, H.; Garrault, S.; Regnaud, L.; Nonat, A. Mechanisms and Parameters Controlling the Tricalcium Aluminate Reactivity in the Presence of Gypsum. *Cem. Concr. Res.* **2007**, *37*, 1418–1426.

(38) Quennoz, A.; Scrivener, K. L. Interactions between Alite and C3A–Gypsum Hydrations in Model Cements. *Cem. Concr. Res.* **2013**, *44*, 46–54.

(39) Garrault, S.; Nonat, A. Hydrated Layer Formation on Tricalcium and Dicalcium Silicate Surfaces: Experimental Study and Numerical Simulations. *Langmuir* **2001**, *17*, 8131–8138.

(40) Bullard, J. W. A Determination of Hydration Mechanisms for Tricalcium Silicate Using a Kinetic Cellular Automaton Model. *J. Am. Ceram. Soc.* **2008**, *91*, 2088–2097.

(41) Bullard, J. W.; Flatt, R. J. New Insights into the Effect of Calcium Hydroxide Precipitation on the Kinetics of Tricalcium Silicate Hydration. *J. Am. Ceram. Soc.* **2010**, *93*, 1894–1903.

(42) Lapeyre, J.; Kumar, A. Influence of Pozzolanic Additives on Hydration Mechanisms of Tricalcium Silicate. *J. Am. Ceram. Soc.* **2018**, DOI: 10.1111/jace.15518.

(43) Allen, A. J.; Thomas, J. J.; Jennings, H. M. Composition and Density of Nanoscale Calcium–silicate–hydrate in Cement. *Nat. Mater.* **2007**, *6*, 311–316.

(44) Thomas, J. J.; Jennings, H. M.; Allen, A. J. Relationships between Composition and Density of Tobermorite, Jennite, and Nanoscale CaO–SiO₂–H₂O. *J. Phys. Chem. C* **2010**, *114*, 7594–7601.

(45) Bentz, D. P.; Lura, P.; Roberts, J. W. Mixture Proportioning for Internal Curing. *Concr. Int.* **2005**, *27*, 35–40.

(46) Nelder, J. A.; Mead, R. A Simplex Method for Function Minimization. *Comput. J.* **1965**, *7*, 308–313.

(47) McKinnon, K. I. M. Convergence of the Nelder–Mead Simplex Method to a Nonstationary Point. *SIAM J. Optim.* **1998**, *9*, 148–158.

(48) Kumar, A.; Oey, T.; Falla, G. P.; Hensensiefken, R.; Neithalath, N.; Sant, G. A Comparison of Intergrinding and Blending Limestone on Reaction and Strength Evolution in Cementitious Materials. *Constr. Build. Mater.* **2013**, *43*, 428–435.

(49) Bentz, D. P.; Garboczi, E. J.; Haecker, C. J.; Jensen, O. M. Effects of Cement Particle Size Distribution on Performance Properties of Portland Cement-Based Materials. *Cem. Concr. Res.* **1999**, *29*, 1663–1671.

(50) Kumar, A.; Oey, T.; Falzone, G.; Huang, J.; Bauchy, M.; Balonis, M.; Neithalath, N.; Bullard, J.; Sant, G. The Filler Effect: The Influence of Filler Content and Type on the Hydration Rate of Tricalcium Silicate. *J. Am. Ceram. Soc.* **2017**, *100*, 3316–3328.

(51) Stoian, J.; Oey, T.; Bullard, J. W.; Huang, J.; Kumar, A.; Balonis, M.; Terrill, J.; Neithalath, N.; Sant, G. New Insights into the Prehydration of Cement and Its Mitigation. *Cem. Concr. Res.* **2015**, *70*, 94–103.

(52) Gallucci, E.; Scrivener, K.; Groso, A.; Stampanoni, M.; Margaritondo, G. 3D Experimental Investigation of the Microstructure of Cement Pastes Using Synchrotron X-Ray Microtomography (MCT). *Cem. Concr. Res.* **2007**, *37*, 360–368.

(53) Jennings, H. M.; Johnson, S. K. Simulation of Microstructure Development during the Hydration of a Cement Compound. *J. Am. Ceram. Soc.* **1986**, *69*, 790–795.

- (54) Powers, T. C. Structure and Physical Properties of Hardened Portland Cement Paste. *J. Am. Ceram. Soc.* **1958**, *41*, 1–6.
- (55) Powers, T. C.; Brownyard, T. L. Studies of the Physical Properties of Hardened Portland Cement Paste. *ACI J. Proc.* **1946**, *43*, 101–132.
- (56) Kumar, A.; Oey, T.; Kim, S.; Thomas, D.; Badran, S.; Li, J.; Fernandes, F.; Neithalath, N.; Sant, G. Simple Methods to Estimate the Influence of Limestone Fillers on Reaction and Property Evolution in Cementitious Materials. *Cem. Concr. Compos.* **2013**, *42*, 20–29.
- (57) Puerta-Falla, G.; Kumar, A.; Gomez-Zamorano, L.; Bauchy, M.; Neithalath, N.; Sant, G. The Influence of Filler Type and Surface Area on the Hydration Rates of Calcium Aluminate Cement. *Constr. Build. Mater.* **2015**, *96*, 657–665.
- (58) Juilland, P.; Kumar, A.; Gallucci, E.; Flatt, R. J.; Scrivener, K. L. Effect of Mixing on the Early Hydration of Alite and OPC Systems. *Cem. Concr. Res.* **2012**, *42*, 1175–1188.
- (59) Banala, A.; Kumar, A. Numerical Simulations of Permeability of Plain and Blended Cement Pastes. *Int. J. Adv. Eng. Sci. Appl. Math.* **2017**, *9*, 67–86.
- (60) Kumar, A.; Reed, J.; Sant, G. Vertical Scanning Interferometry: A New Method to Measure the Dissolution Dynamics of Cementitious Minerals. *J. Am. Ceram. Soc.* **2013**, *96*, 2766–2778.
- (61) Garrault-Gauffinet, S.; Nonat, A. Experimental Investigation of Calcium Silicate Hydrate (C-S-H) Nucleation. *J. Cryst. Growth* **1999**, *200*, 565–574.
- (62) Garrault, S.; Finot, E.; Lesniewska, E.; Nonat, A. Study of C-S-H Growth on C3S Surface during Its Early Hydration. *Mater. Struct.* **2005**, *38*, 435–442.
- (63) Juilland, P.; Gallucci, E.; Flatt, R.; Scrivener, K. Dissolution Theory Applied to the Induction Period in Alite Hydration. *Cem. Concr. Res.* **2010**, *40*, 831–844.
- (64) Bazzoni, A.; Cantoni, M.; Scrivener, K. L. Impact of Annealing on the Early Hydration of Tricalcium Silicate. *J. Am. Ceram. Soc.* **2014**, *97*, 584–591.
- (65) Damidot, D.; Nonat, A.; Barret, P. Kinetics of Tricalcium Silicate Hydration in Diluted Suspensions by Microcalorimetric Measurements. *J. Am. Ceram. Soc.* **1990**, *73*, 3319–3322.
- (66) Bellmann, F.; Damidot, D.; Möser, B.; Skibsted, J. Improved Evidence for the Existence of an Intermediate Phase during Hydration of Tricalcium Silicate. *Cem. Concr. Res.* **2010**, *40*, 875–884.
- (67) Zhang, J.; Weissinger, E. A.; Peethamparan, S.; Scherer, G. W. Early Hydration and Setting of Oil Well Cement. *Cem. Concr. Res.* **2010**, *40*, 1023–1033.
- (68) Kumar, A.; Oey, T.; Kim, S.; Thomas, D.; Badran, S.; Li, J.; Fernandes, F.; Neithalath, N.; Sant, G. Simple Methods to Estimate the Influence of Limestone Fillers on Reaction and Property Evolution in Cementitious Materials. *Cem. Concr. Compos.* **2013**, *42*, 20–29.
- (69) Garrault, S.; Behr, T.; Nonat, A. Formation of the C–S–H Layer during Early Hydration of Tricalcium Silicate Grains with Different Sizes. *J. Phys. Chem. B* **2006**, *110*, 270–275.
- (70) Lothenbach, B.; Winnefeld, F. Thermodynamic Modelling of the Hydration of Portland Cement. *Cem. Concr. Res.* **2006**, *36*, 209–226.
- (71) Brown, P. W.; Franz, E.; Frohnsdorff, G.; Taylor, H. F. W. Analyses of the Aqueous Phase during Early C3S Hydration. *Cem. Concr. Res.* **1984**, *14*, 257–262.
- (72) Brown, P. W.; Harner, C. L.; Prosen, E. J. The Effect of Inorganic Salts on Tricalcium Silicate Hydration. *Cem. Concr. Res.* **1986**, *16*, 17–22.
- (73) Ahmed, H.; Buckton, G.; Rawlins, D. A. The Use of Isothermal Microcalorimetry in the Study of Small Degrees of Amorphous Content of a Hydrophobic Powder. *Int. J. Pharm.* **1996**, *130*, 195–201.
- (74) Darcy, P.; Buckton, G. Quantitative Assessments of Powder Crystallinity: Estimates of Heat and Mass Transfer to Interpret Isothermal Microcalorimetry Data. *Thermochim. Acta* **1998**, *316*, 29–36.
- (75) Zhang, J.; Scherer, G. W. Comparison of Methods for Arresting Hydration of Cement. *Cem. Concr. Res.* **2011**, *41*, 1024–1036.